BNL-79807-2008-JA

A TECHNIQUE FOR THE AUTOMATIC DETECTION AND REMOVAL OF INSECT CLUTTER IN CLOUD RADAR RETURNS

E. P. Luke, P. Kollias, K. L. Johnson, and E. E. Clothiaux

January 2008

For publication in
J. Atmos. Oceanic Technol.
(in press)

Environmental Sciences Department/Atmospheric Sciences Division

Brookhaven National Laboratory
P.O. Box 5000
Upton, NY 11973-5000
www.bnl.gov

Notice: This manuscript has been authored by employees of Brookhaven Science Associates, LLC under Contract No. DE-AC02-98CH10886 with the U.S. Department of Energy. The publisher by accepting the manuscript for publication acknowledges that the United States Government retains a non-exclusive, paid-up, irrevocable, world-wide license to publish or reproduce the published form of this manuscript, or allow others to do so, for United States Government purposes.

DISCLAIMER

This report was prepared as an account of work sponsored by an agency of the United States Government. Neither the United States Government nor any agency thereof, nor any of their employees, nor any of their contractors, subcontractors, or their employees, makes any warranty, express or implied, or assumes any legal liability or responsibility for the accuracy, completeness, or any third party's use or the results of such use of any information, apparatus, product, or process disclosed, or represents that its use would not infringe privately owned rights. Reference herein to any specific commercial product, process, or service by trade name, trademark, manufacturer, or otherwise, does not necessarily constitute or imply its endorsement, recommendation, or favoring by the United States Government or any agency thereof or its contractors or subcontractors. The views and opinions of authors expressed herein do not necessarily state or reflect those of the United States Government or any agency thereof.

A Technique for the Automatic Detection and Removal of Insect Clutter in Cloud Radar Returns

Edward P. Luke[1], Pavlos Kollias[1], Karen L. Johnson[1] and Eugene E. Clothiaux[2]

1. Atmospheric Sciences Division, Brookhaven National Laboratory
2. Department of Meteorology, Pennsylvania State University

Corresponding author:
Edward P. Luke,
Atmospheric Sciences Division,
Brookhaven National Laboratory
Bldg 490D, Bell Ave.
Upton NY, 11973
Email: eluke@bnl.gov

Abstract

The United States Department of Energy Atmospheric Radiation Measurement (ARM) program operates 35-GHz millimeter-wavelength cloud radars (MMCRs) in several climatologically distinct regions. The MMCRs, centerpiece instruments for the observation of clouds and precipitation, provide continuous, vertically-resolved information on all hydrometeors above the ARM Climate Research Facilities (ACRF). However, their ability to observe clouds in the lowest 2-3 km of the atmosphere is often obscured by the presence of strong echoes from insects, especially during the warm months at the continental mid-latitude Southern Great Plains (SGP) ACRF. Here, a new, automated technique for the detection and elimination of insect echoes from the MMCR observations is presented. The technique is based on recorded MMCR Doppler spectra, a feature extractor that conditions insect spectral signatures and the use of a neural network algorithm for the generation of an insect (clutter) mask. The technique exhibits significant skill in the identification of insect radar returns (more than 92% of insect-induced returns are identified) when the sole input to the classifier is the MMCR Doppler spectrum. The addition of circular polarization observations by the MMCR and ceilometer cloud base measurements further improve the performance of the technique and form an even more reliable method for the removal of insect radar echoes at the ARM site. Recently, a 94-GHz Doppler, polarimetric radar was installed next to the MMCR at the ACRF SGP site. Observations by both radars are used to evaluate the potential of the 94-GHz as an insect-free radar and show that dual wavelength radar reflectivity measurements can be used to identify insect radar returns.

1. INTRODUCTION

During the past 20 years, there has been substantial progress in the development and application of millimeter-wavelength radars in atmospheric research (Kollias et al., 2006a). Their short wavelengths (3 mm and 8.6 mm, corresponding to frequencies of 94- and 35-GHz, respectively) allow these radars to detect clouds with small droplets or ice crystals at high spatial and temporal resolution and infer important information on their microphysical and dynamical structure (e.g., Lhermitte, 1987; Frisch et al., 1995; Kollias and Albrecht, 2000; Sassen et al., 2000; Hogan et al., 2005). Although cloud radars are insensitive to Bragg scattering in the lower troposphere, hydrometeors are not their only source of atmospheric backscatter. Small insects produce strong radar echoes in the lowest 2-3 km of the atmosphere (e.g., Clothiaux et al., 2000; Geerts and Miao, 2005), especially over land and during the warm season. These insect radar echoes in the boundary layer have reflectivities comparable to those of clouds and precipitation, and contaminate and mask the true cloud returns, making detection of cloud base difficult without the use of a laser instrument. Insect radar echoes ("atmospheric plankton", Lhermitte, 1966) are not new to radar meteorologists and in some cases can be used as a tracer of the wind field at low levels in scanning weather radar applications (e.g., Vaughn, 1985; Achtemeier, 1990; Wilson et al., 1994).

The United States (US) Department of Energy (DOE) ARM program operates a network of millimeter-wavelength cloud radars (MMCRs; Moran et al., 1998) in several climatological regimes (Clothiaux et al., 2000). These cloud radars are one of the primary observing tools for quantifying the properties of nearly all radiatively important clouds over the ARM Climate Research Facilities (ACRF; e.g., Ackerman and Stokes, 2003).

Clothiaux et al. (2000) show that about 90% of the radar range gates in the boundary layer are contaminated by insect clutter during June through August at the ARM site in Oklahoma. This limits our ability to sample properly boundary layer clouds and to assess accurately the role of these clouds in Earth's radiation budget. Thus, the accurate detection and removal of insect clutter from millimeter-wavelength cloud radar (MMCR) returns is of high importance to ARM program boundary layer cloud research.

In this study we look beyond traditional Doppler radar moments to ask whether analysis of recorded Doppler spectra can serve as the basis for reliable, automatic insect clutter screening. We focus on the MMCR operated at the Southern Great Plains (SGP) ACRF in Oklahoma. Here, archiving of full Doppler spectra began in September 2003, and the pronounced insect presence regularly introduces clutter into boundary layer returns. The Doppler spectrum signatures of insects have characteristics that differ from those of cloud and precipitation particles. We are able to enhance these differences by applying an appropriate feature extractor to the recorded Doppler spectra and input the features to a neural network to classify each range gate as insect contaminated or not.

Recently (fall of 2005), a 94-GHz Doppler, polarimetric radar was installed next to the MMCR at the SGP ACRF. Insect observations from both radars are used to evaluate the potential of the 94-GHz radar as an insect-free one. When these two radars are collocated, dual wavelength radar reflectivity measurements can be used to identify insect radar returns.

2. BACKGROUND

Since the beginning of MMCR observations at the SGP ACRF (November 1996) it was evident that insect radar returns pose a serious obstacle in our effort to detect boundary layer clouds. Insect clutter is a common year-round occurrence at the SGP ACRF, even during the winter months. For example, insect returns were observed on 85% of the days from January 1st through March 21st, 2006. Similar insect-induced radar echoes have been frequently observed at other ARM sites, especially in the tropics (e.g., Darwin, Australia), and the European CloudNet sites (e.g., Chilbolton, United Kingdom). Insects have radar reflectivities comparable to those from typical boundary layer clouds and Doppler velocities that are a combination of the vertical air motion and their own motion (Geerts and Miao, 2005). If only MMCR Doppler moments (reflectivity, mean Doppler velocity and Doppler spectrum width) are provided, it is difficult to achieve a reliable screening of insect clutter from cloud returns since their Doppler moment distributions overlap. Screening of profiling cloud radar insect clutter has historically involved a laborious manual process of cross-referencing radar moments against measurements from other collocated instruments, such as the ceilometer (Clothiaux et al., 2000).

During the Single Column Modeling/Cloud Intensive Observing Period (IOP, 27 April to 17 May 1998) at the SGP ACRF, in situ samples of airborne insects were collected. Using a remotely operated capture device (Ben Balsley, personal communication) flown from a tethered balloon and parafoil kite, insects were collected between the surface and 700 m above ground level during several days of the IOP. For a typical flight approximately 70 insects were collected during one hour at several hundred meters altitude. This equates to roughly one insect per MMCR range gate most of the time. The

physical characteristics of the average insect were a wing length of 4-5 mm, a wing width of 1-2 mm and a body length of 2 mm, suggesting the presence of non-Rayleigh scattering at millimeter wavelengths.

A typical example of MMCR insect radar returns on a cloud-free day is shown in Fig. 1. The atmospheric plankton (insect layer, Lhermitte, 1966) covers the lower 1-2 km of the atmosphere. At 35-GHz, the insect radar reflectivity distribution covers a wide range (-35 dBZ to 0 dBZ) and the texture of the insect layer exhibits great variability. Radar returns from non-precipitating and precipitating stratus and broken cumuli cover a similar range. The depth of the insect layer follows the diurnal variation of the convective boundary layer with a minimum during nighttime, sharply increasing during the morning and reaching a maximum in the afternoon. Figure 2. shows hourly average temperature for the month of May 2005 at 60 m altitude, along with hourly average insect column height for the same period. The hourly average temperatures are highly correlated with the height of the insect column.

To demonstrate further that temperature is a strong controlling factor in insect layer presence and depth consider Fig. 3a. This figure shows insect layer top height and the 10 °C isotherm height from soundings. Their Pearson product-moment correlation coefficient is 0.67. The Pearson product-moment correlation coefficient of two variables X and Y is defined as their covariance divided by the product of their standard deviations:

$$\mathrm{Cov}(X,Y) / (\sigma(X)\, \sigma(Y))$$

We find that the 10 °C isotherm height can be used as an approximation for the ceiling of

the insect layer in most cases. A similar finding on the relationship between insect presence in the boundary layer and temperature was found by Khandwalla et al. (2002). We do find exceptions to this rule, one of which appears to be a willingness of insects to tolerate lower temperatures after prolonged periods of lower than average and, especially, sub-freezing temperatures.

To gain a better sense of this relationship we identified a set of twenty one days from November 2005 through April 2006 with hourly averaged temperatures between 20:00 UTC and 21:00 UTC (14:00 to 15:00 local standard time) falling into bins ranging from 0 °C to 20 ºC in 1 ºC increments (Table 1). Our choice of the period 20:00 UTC to 21:00 UTC was guided by the observation that both the hourly average temperature and insect coverage reach their peaks near this time of day (Fig. 2.). For consistency, when multiple days were available for a given temperature bin, we always chose the day with the least cloud cover. For each chosen day, we computed the fractional insect coverage averaged over the 2nd and 3rd range gates (150 m and 195 m) from the ground. Figure 3b shows that the fractional coverage near the surface can be predicted on the basis of temperature (T) in degrees centigrade by a sigmoid logistic function as follows:

$$f = \frac{1}{1 + e^{\frac{10-T}{2}}}$$

This model predicts a 50% probability of insect occurrence per range gate at a temperature of 10 °C, with a sharp fall-off at decreasing temperatures. Thus, near the ground, 10 °C seems to be an approximate threshold temperature as to whether insects decide to take flight on a given day. Geerts et al., (2005) show that insects may seek updrafts opportunistically to augment their own mobility. We see possible evidence of

this as well. Figure 3c shows the distribution of insect (vertical) mean Doppler velocities for May 5, 2005, at the SGP ACRF. The bimodality suggests two organized sets of behaviour with a preference for ascent at roughly 0.1 m s^{-1}.

During the ARM multi-frequency radar IOP in 2001, a 94-GHz vertically-pointing Doppler radar was deployed next to the MMCR to evaluate whether the 94-GHz radar cloud measurements are less affected by insect clutter (Khandwalla et al., 2001; 2002). The analysis revealed that the MMCR (35-GHz) insect reflectivities are consistently higher by about 20 dB than the 94-GHz insect reflectivities. The use of polarimetric filtering of insect returns was also explored at the ARM site. The findings suggest that both linear and circular polarization millimeter-wavelength radar measurements could offer a means of distinguishing between cloud droplets and insects (Sekelsky et al., 1998; Martner and Moran, 2000). However, this requires the extensive use of a polarization mode at the expense of valuable cloud information.

In 2003, ARM initiated an upgrade of the MMCR digital signal processors to allow for enhancements to their operational parameters (Clothiaux et al., 2000; Kollias et al., 2005). The new sampling strategy for the ARM profiling clouds radars (Kollias et al., 2006b) includes significant improvement in temporal resolution (i.e., less than 1 s for dwell and 2 s for dwell and processing), wider Nyquist velocities, operational de-aliasing of the recorded spectra, removal of pulse compression while sampling the boundary layer, and continuous recording of 128 and 256-point FFT Doppler spectra. The MMCR Doppler spectrum reports the distribution of the return echo over a range of Doppler velocities. Although the main objective of Doppler spectra recording is the extraction of

information relevant to the microphysical and dynamical content of the observed cloud and precipitation conditions at the ARM sites, we investigate here the potential for accurate identification of insect clutter returns from the recorded Doppler spectra. In the following sections we will present our automated algorithm for the detection of insect returns (section 3), examples of insect masks that illustrate its potential (section 4) and discuss the potential of a 94-GHz cloud radar as an insect-free radar.

3. INSECT DETECTION ALGORITHM USING DOPPLER SPECTRA

Our primary objective was to develop an automatic spectrum analysis tool for generating masks of insect clutter that is solely based on recorded Doppler spectra. Such an algorithm is described here and it will be applied to all the ACRF (35- and 94-GHz) cloud radars that suffer from strong returns from insects. The algorithm is applicable to all profiling radars that record Doppler spectra with adequate spectral velocity resolution (better than 10 cm s^{-1}).

The body and wing motions of airborne insects produce Doppler radar spectra with morphologies that are often distinguishable by eye from those of clouds. This led us to develop a signal processing methodology that makes this distinction as well. Doppler spectra from range gates that have a contribution from insects have distinct features (e.g., Fig. 4) that are used by our algorithm for the classification of cloud, insect and mixed returns.

The fundamental morphology of insect-generated Doppler spectra is a sharp narrow peak,

as shown in Fig. 4a. Figures 4a--h are also examples of insect-generated spectra. It is not difficult to visualize these as composed of scaled super-positions of Fig. 4a. Despite their great diversity, we have found insect clutter returns in the SGP ACRF MMCR to contain consistently spiked sub-peaks with sharp roll-offs. The number of sub-peaks appears to be related to the density of the insect layer. More specifically, our analysis indicates that multi-peaked spectra are significantly more probable in higher insect density neighborhoods, leading us to speculate that, at least to some extent, peaks can be mapped to individual insects occupying a range gate. To demonstrate this we computed for each range gate from 01:00 UTC to 02:00 UTC (19:00 to 20:00 local standard time) on February 1, 2006 the insect return density, which we defined as the fraction of insect-containing range gates in a surrounding 5 by 5 time-height neighborhood of range gates. We then separated range gates into single- and multi-peaked groups and for each group computed the cumulative distributions of insect return density (Fig. 5). The distribution of multi-peaked range gates is concentrated toward the higher insect return densities.

In addition to the goal of identifying insects near the ground in fair weather, we are interested in finding insects embedded within clouds, above clouds, and immersed in precipitation. Considering the spectral complexity associated with a dense cloud of insects, particularly ones embedded within cloud, we anticipated that effective characterization of the typically busy spectral fluctuations involved would be one key to success. Since many cases exist where morphological differences between insect and hydrometeor spectra are less than obvious, we sought a technique that operates on the basis of statistical best estimates and adopted a neural network approach. Neural networks are well suited to 256-FFT point Doppler spectra (e.g., Kosko, 1992), which is

the size of spectra from the boundary layer mode of the MMCR at the SGP ACRF.

In this study we used a feed-forward neural network architecture and the back-propagation of error training algorithm. At the top level, our system is comprised of three main functional blocks (Fig. 6a). The first of these is a feature extractor that receives the raw Doppler spectra (64-, 128- or 256-FFT points for the MMCR operational settings) and transforms their information content into a form that is more expressive of the problem domain. To remove unwanted noise, spectra with 256 elements are initially smoothed by a 5-element box-car window filter and spectra with 128 or 64 elements by a 3-element window filter. Since the spectra of radar echoes containing insects typically change quickly with Doppler velocity (i.e., FFT bin), we need as input to the neural network a measure of spectrum morphology that is sensitive to sharp roll-offs. Doppler velocity itself is not well-correlated with the presence of insects so features should be insensitive to it (Morse et al., 2002). We define positive velocity as downward throughout this paper.

The feature extractor generates outputs which are fed to the second main functional block, a feed-forward neural network (Fig. 6a). The output from the neural network is a continuous-valued vector with a component for each possible classification. The outputs range from 0.0 to 1.0, expressing in parallel the confidence of spectrum membership in each class. The third main functional block, the decision criterion, is simply a method of interpreting the neural network output vector and converting it into a discrete decision state. In our case it is the “winner-take-all” function, choosing the output with the highest value as the spectrum classification. The four neural network outputs are clear air, cloud,

precipitation, and insects. In the results presented here we merged the cloud and precipitation classes into a single hydrometeor class.

The feature extractor (Fig. 6b) can itself be broken down into a set of smaller functional units. Of central importance amongst the feature extractor's outputs are frequency of occurrence distributions of the first and second derivatives of the Doppler spectra primary peaks. Figure 7 illustrates the processing steps to arrive at these distributions using insect and cloud Doppler spectra. To begin each Doppler power spectrum (Fig. 7a) is stripped of content not belonging to its primary peak (Fig. 7b) based on a noise floor computed with the Hildebrand-Sekhon method (Hildebrand and Sekhon, 1974; Kollias, et al., 2007), and applied to the input of the feature extractor. The primary peak's first and second derivatives (Figs. 7c and d) are computed at each point, and each is accumulated into a fifty-bin histogram, labeled H2 and H1 (in Fig 6b), covering a range of -5.0 to 5.0 dB/bin and dB/bin^2, respectively (Figs. 7e and f). The examples shown in Fig. 7 illustrate the differences in the frequency of occurrence distributions of spectral derivatives from cloud and insect Doppler spectra. Collectively, the outputs of the two histograms provide 100 of the feature extractor's 112 outputs, and thus convey the bulk of the spectral morphology information to the neural network.

The feature extractor also contains two low-pass filters (LPF) that successively smooth the input power spectrum of the primary peak. The differences between the smoothed and original spectra are integrated and applied as two inputs to the neural network, as a measure of overall spectrum high frequency content. The average power within the primary peak is also applied as a neural network input. Spectral width (σ), mean Doppler

velocity (<V>), skewness (S(V)), and kurtosis (K(V)) of the primary peak, as well as target range (r), are applied to the neural network to take advantage of any secondary information they might convey. Three inputs labeled “64”, “128”, and “256” inform the neural network as to the number of bins in the original spectrum. Thus far, we have only used 256 element spectra, which is the number of FFT points used in the MMCR boundary layer mode. Finally, day of the year (JD) is input to enable seasonal variations to be incorporated into the neural network's training. For this study we kept the seasonal inputs constant, but may explore their utility in the future. A modest-sized data set comprising 2000 Doppler spectra samples from each of the four classes (clear, cloud, precipitation, and insects) was used to train the classifier (Table 2).

4. RESULTS

The insect/hydrometeor classifier output is evaluated against MMCR polarimetric measurements and ceilometer cloud base. A polarization mode was installed on the SGP ACRF MMCR (August 2004) that provides co- and cross-channel Doppler spectra and moments (Kollias et al., 2006). During the polarization mode, returns from (right hand) circularly polarized transmitted signals are received by both left hand (co-channel) and right hand (cross-channel) circular receivers on a pulse-to-pulse basis. Utilizing the less negative circular depolarization ratios (CDRs), defined as the ratio of power received in the cross-channel to that received in the co-channel, of non-spherical scatterers (e.g., insects), the polarization mode can be useful for identifying insects in the boundary layer. For the SGP ACRF MMCR several problems limit the use of CDR for identification of

insects. First, the poor antenna cancellation ratio (13-15 dB) of the MMCR imposes limitations on the use of CDR for identifying insects in radar returns. Second, the coarse temporal sampling interval (30 s) and spatial resolution (90 m) of the MMCR polarization mode further limits its use for insect detection.

Figure 8a shows the frequency of occurrence histogram of MMCR CDR observations in the boundary layer for the entire month of May 2005. The left peak corresponds to spherical scatterers, which we take to be hydrometeors, and the right to non-spherical, which we assume are insects. We find this pattern of bimodality to occur ubiquitously throughout the MMCR data archive regardless of timeframe, as long as insect and hydrometeor returns are captured in the same sample set. It is beyond the scope of this study to determine whether insects avoid clouds, possibly enhancing the separation of these peaks. However, CDR values attributable to spherical hydrometeors dictate that very little power be received in the radar's cross-polarized channel. Even a small contribution of power to the cross-polarized channel from an insect embedded in a cloud will strongly swing the net CDR in a positive direction, in most cases well past the valley located around -10dB and into the right-hand peak.

The CDR measurements of spherical hydrometeors (i.e., cloud and drizzle droplets) are concentrated around -15 dB in accordance with the MMCR's antenna cancellation ratio. We run the insect/hydrometeor classifier for the same period (May 2005) and subset the CDR values into two groups according to our classifier's insect/hydrometeor output (Fig. 8b). The resulting CDR frequency of occurrence distributions for insects and hydrometeors have good separation. Using a CDR threshold of -10.5 dB, the classifier

successfully classifies an insect radar return as insect 92.7% of the time and a hydrometeor radar return as hydrometeor 86.9% of the time.

The misclassification of hydrometeor radar returns as insects by the Doppler spectra-based classifier is further explored. Figure 9 shows classification accuracies of insects and hydrometeors as a function of the spectral width of the primary peak. For spectral widths less than 0.2 m s^{-1} the overwhelming probability is for the return to be from insects. This, plus the similar morphologies of narrow insect and hydrometeor spectra makes identification of hydrometeor returns with narrow spectral widths difficult. Additional analyses indicated that the misclassifications are not random range gates in cloudy areas. They are coherent structures that coincide with the presence of very low turbulence (quiet-air) conditions in clouds (e.g., Gossard et al., 1997). Such conditions are not frequently observed in boundary layer clouds. When they do occur, the result is minimum turbulence spectral broadening and very low Doppler spectral widths (e.g., Kollias et al., 2001). Thus, we attribute a large portion of the misclassifications to confusion between narrow single-insect clutter and narrow hydrometeor Doppler spectra peaks in quiet air conditions.

Since most of the hydrometeor radar returns misclassified as insects have narrow Doppler spectra width (less than 0.2 m s^{-1}) and very low radar reflectivity, we added a post-classifier criterion to minimize these misclassifications. If the Doppler spectrum width is less than 0.2 m s^{-1} and the classifier output is insect, the nearest (in time and height) CDR value is considered. If the CDR value is greater than -10.5 dB (non-spherical particle return) the decision state remains, otherwise the decision state is reversed. The addition

of this post-classifier criterion improved the accuracy of hydrometeor classification to approximately 95%.

Figure 10a shows a time-height mapping of MMCR radar reflectivity for several days in May 2005, with a gap in the MMCR observations between May 10 and 11, 2005. The temporal resolution is 4 s and the spatial resolution is 45 m. During this period, substantial presence of insects with embedded boundary layer clouds and precipitation is observed. The top of the insect layer fluctuates between 1 km and 2 km and there is poor separability of insects from hydrometeors in the radar reflectivity image. In the absence of insects the MMCR (Moran et al., 1998) is capable of detecting clouds in the boundary layer with reflectivities as low as -50 dBZ. The presence of insects in the boundary layer generates a MMCR minimum detectable signal of -10 dBZ to -5 dBZ for hydrometeors. That is, the presence of insects impedes the detection of hydrometeors that do not produce radar reflectivities substantially higher than those from insects, with maximum values around -10 dBZ to -5 dBZ.

The hydrometeor/insect classification mask produced by the Doppler spectra-based insect detection algorithm for the same period in May 2005 is shown in Fig. 10b. The classification mask has three different classes: insects, hydrometeors (i.e., combined cloud and rain classes) and the CDR reclassified class, which contains samples initially classified as insect that were relabelled as hydrometeor using the CDR observations. The classifier produces structures of hydrometeors which are cohesive in time and space and consistent with ceilometer cloud base detections.

Ceilometers can be used to identify the presence of insects and clouds in the boundary layer. The concentration of insects is several orders of magnitude lower than the concentration of cloud droplets and, as such, a ceilometer will only detect a hydrometeor layer. If a ceilometer detects no cloud base height in the boundary layer, all the radar echoes are generated by insects. Accordingly, if the ceilometer detects a cloud base, the radar echoes below the ceilometer cloud base height can be attributed to insects and the radar echoes above the cloud base height can be attributed to hydrometeors. This radar/lidar approach is used to remove non-hydrometeor radar returns in the Active Remote Sensing of CLouds (ARSCL) product (Clothiaux et al., 2000). ARSCL processes data from multiple instrument types to derive a best estimate of cloud location and boundaries. This approach, which requires laser-derived cloud base heights, assumes that radar echoes below ceilometer cloud base are from hydrometeors only if the below cloud reflectivities are greater than temporally surrounding values from any known insects and no insects are above the ceilometer cloud base height, which is often not the case for shallow broken clouds. As a result, the screening of radar insect clutter has historically involved a laborious semi-automated process of cross-referencing radar moments against measurements from other collocated instruments, such as ceilometer and lidar (Clothiaux et al., 2000).

Significant improvements in automatic cloud mask generation in insect-contaminated boundary layers are possible with the new automated Doppler spectra-based algorithm. Figure 11a shows two examples of boundary layer MMCR radar reflectivities: a four hour period (18:00--22:00 UTC or 12:00--16:00 local standard time) on May 5, 2005, and a twelve hour period (12:00--24:00 UTC or 6:00—18:00 local standard time) on May 12,

2005. In both cases, clouds and insects are present in the boundary layer. The cloud mask produced by ARSCL and the ceilometer cloud base are shown in Fig. 11b. The current ARSCL mask heavily depends on the detection of a cloud base height from the ceilometer or micropulse lidar. For the May 5 case all MMCR radar reflectivities above the ceilometer cloud base are flagged by ARSCL as hydrometeor candidate echoes. Before 14:00 UTC on May 12, all MMCR radar reflectivities above the ceilometer cloud base are also flagged by ARSCL as hydrometeor candidate returns. On May 12 radar reflectivities below the ceilometer base are also included in the ARSCL hydrometeor mask, as precipitating size particle radar returns between 22:00-24:00 UTC produce radar reflectivities greater than those from nearby (in time and space) insects.

The hydrometeor/insect classification masks produced by the Doppler spectra-based insect detection algorithm for the same time periods are shown in Fig. 11c. For May 5 the classifier is able to detect the shallow liquid layer embedded in the insect layer and the range of heights of the liquid layer is consistent with the ceilometer cloud base heights. Relative to the Doppler spectra-based classifier, the ARSCL mask overestimates the vertical thickness and cloud fraction of the hydrometeor layer, exemplifying one limitation of the current ARSCL scheme in cases where insects are present at the tops of hydrometeor layers. For the May 12 case the classifier maps accurately the cloud amount and boundaries, preserving the precipitation returns from 22:00-24:00 UTC that are below ceilometer cloud base. Taken together, these two results indicate that the current approach is a viable one for replacing the ARSCL algorithm and thereby removing the necessity of the two assumptions embedded in the ARSCL algorithm that we described above.

5. 94-GHz RADAR OBSERVATIONS OF INSECTS

During previous field experiments at the SGP ACRF (e.g., fall 1997 Cloud IOP, 2001 Multi-Frequency Radar IOP), 94-GHz radars were collocated with the ARM 35-GHz MMCR (e.g., Sekelsky et al., 1998; Khandwalla et al., 2001). Measurements from these IOPs indicated that insect radar returns at 94-GHz are almost 20 dB lower than corresponding measurements at 35-GHz. Non-Rayleigh scattering by insects (i.e., scattering by particles not small compared to the wavelength) at millimeter-wavelengths can explain the observed Dual-Wavelength Ratio (DWR) values from insects at the two radar frequencies. Scattering of liquid cloud droplets at millimeter wavelength falls in the Rayleigh scattering regime (i.e., scattering by particles small compared to the wavelength), leading to identical radar reflectivities at the two wavelengths and DWR values of zero. Khandwalla et al. (2003) developed insect filters based on the linear depolarization ratio (LDR) at 94-GHz and applied to data for which DWR values were also available. LDR is defined to be the ratio of cross-polarized received power to co-polarized received power for a radar with dual-channel linear polarization. The findings of these studies indicated that 94-GHz radars are less sensitive to insects and that DWR measurements at 35- and 94-GHz and LDR measurements at 94-GHz can be used for distinguishing clouds from insects in the boundary layer.

In 2005, a highly sensitive ground-based polarimetric 94-GHz Doppler radar was deployed to the SGP ACRF (Mead and Widener, 2005). This 94-GHz radar incorporates the latest technological developments in millimeter-wavelength radar design, records

Doppler spectra, and measures LDR. It was placed at the SGP ACRF to help resolve the insect problem in the boundary layer. Examples of insect returns from both radars are shown in Fig. 12. On May 19, 2006, the ceilometer detected no cloud base, the microwave radiometer detected no liquid water, and the total sky imager (Long et al., 2001) hemispherical pictures of the sky show no evidence of clouds. Insects are clearly the only scatterers at radar wavelengths in the boundary layer on this day. The morphology of the insect layer from the two radars is similar, with the top of the insect layer higher at 35-GHz by an average of 100--300 m relative to that at 94-GHz. Nonetheless, the 94-GHz radar detects many insects in the boundary layer, making it difficult to discriminate clouds from insects using 94-GHz radar reflectivities.

This last finding is not consistent with previous 94-GHz radar observations of insects at the SGP ACRF. It is due to the greater sensitivity of the 94-GHz recently deployed at the SGP ACRF as compared to the 94-GHz radars used in the previous field experiments (e.g., fall 1997 Cloud IOP, 2001 Multi-Frequency Radar IOP). Due to non-Rayleigh scattering, the insect returns at 94-GHz are suppressed by 20 dB on average compared to the same insect returns at 35-GHz (Fig. 13a). The 94-GHz radars deployed at the SGP ACRF in the past had an average sensitivity of -30 dBZ to -33 dBZ at 1 km height. As a result, only a small portion of the observed insect reflectivities in Fig. 13a would have been observed by them. The 94-GHz radar now at the SGP ACRF has an average sensitivity of -50 dBZ at 1 km height and a much larger number of (previously undetected) insect radar returns are observed. As a result, though the contrast between cloud and insect radar reflectivities at 94-GHz is enhanced (i.e., improved hydrometeor to clutter return ratio), it is not sufficient to separate hydrometeors from insects.

We also examined the use of 94-GHz LDR as a basis for filtering the insect returns in the boundary layer (Khandwalla et al., 2003). Fig. 13b shows the LDR frequency of occurrence distribution for May 21, 2006, a day that included both cloud and insect radar returns. The polarization isolation of the 94-GHz antenna is around -26 dB, allowing the measurement of very low LDR values. Two different cloud masks are used, one based on co-polar channel signal-to-noise ratios (SNRs) and the other based on cross-polar channel signal-to-noise ratios. As Fig. 13b illustrates, the insect LDR distribution covers values from -35 dB to +10 dB with a primay peak at -10 dB, depending on insect size and shape. The secondary peak at -26 dB is the hydrometeor LDR distribution and its position depends on the antenna polarization isolation. Ideally, we would like to have a better antenna polarization ratio (e.g., -35 dB) to create better separation between the insect and hydrometeor LDR distributions.

As it is, the overlap of the LDR distributions suggests that it is not feasible to create an insect filter that is solely LDR-based. Also, LDR is not measurable at low signal-to-noise ratio conditions. Nonetheless, LDR measurements could be part of a conditional insect filtering algorithm that includes other inputs, such as DWR or the Doppler spectra-based classifier output.

6. SUMMARY

Uncertainty about the possible presence of insect clutter in cloud profiling Doppler radar returns is a hindrance to boundary layer cloud research in climates and seasons where insects are prevalent. This is particularly true in radiative transfer and cloud

parameterization studies for which liquid cloud layer thicknesses and fractions are of high importance. We have developed a new technique that extracts an indication of insect clutter primarily from Doppler spectrum morphologies, mitigating a deficiency in the ability of current profiling methods to locate accurately cloud boundaries in many situations where insects are present. The algorithm is applicable to all profiling radars that record Doppler spectra with adequate spectral velocity resolution (better than 10 cm s^{-1}) to preserve the narrow spectral signatures of insects.

The technique is based on recorded Doppler spectra, a feature extractor that conditions insect spectral signatures and the use of a neural network algorithm for the generation of an insect (clutter) mask. Perhaps the most important features in the current approach are frequency of occurrence histograms of spectral first and second derivatives, since insect and cloud spectra possess different slopes and concavities. These features form the basis for about 90% of our input to the neural network. Other features extracted from the spectra are the average received power, spectral width, mean Doppler velocity, skewness, kurtosis, and a measure of overall high frequency content. Finally, we include range gate altitude and day of the year in order to capture possible altitude- and time-dependent insect effects.

The classifier successfully classifies an insect radar return as insect 92.7% of the time and a hydrometeor radar return as hydrometeor 86.9% of the time. The addition of a CDR-based post-classifier filter further improves the accuracy of hydrometeor classification to approximately 95%. The classifier exhibits operational stability and does not require any

assumptions on the vertical extent of the insect layer, its presence, or not, above a low-level cloud layer and does not depend on ceilometer data. Thus, it improves upon the current cloud masking technique in the boundary layer, which depends heavily on the detection of cloud base height by a ceilometer and assumptions on the vertical extent and location of insects.

Observations from a 94-GHz radar recently installed at the SGP ACRF demonstrate that 94-GHz radars detect significant amounts of insect return. Previous assessments, which indicated that 94-Ghz radars detect fewer insects, were based on observations collected with radars with limited sensitivity that missed insect radar returns (due to non-Rayleigh scattering) below the radar noise. We found that 94-GHz LDR measurements, by themselves, are not sufficient to filter insect radar returns. The use of a polarization mode in millimeter-wavelength radar research for the filtering of insect returns is not a good practice because these measurements occur at the expense of other valuable cloud observations. DWR measurements have the potential to discriminate hydrometeor and insect returns but require the presence of two radars. In contrast, the Doppler spectra-based algorithm for the discrimination of hydrometeor from insect returns requires only the recording of Doppler spectra and neither polarization nor DWR measurements. The algorithm is applicable to all profiling radars that record Doppler spectra with adequate spectral velocity resolution (better than 10 cm s^{-1}) to preserve the narrow spectral signatures of insects.

Success of the current Doppler spectra-based approach for identifying insect returns holds promise for further classification of radar returns in terms of cloud and rain

properties. The implication is that efficient radar quality control algorithms with less dependence on multiple data streams are possible, as are algorithms that generate a much richer set of cloud classification masks tailored for the specific objectives of specialized research projects.

7. ACKNOWLEDGEMENTS

Support for this research was funded in part by the Atmospheric Sciences Division of the U.S. Department of Energy (under Grant DE-FG02-90ER61071).

8. REFERENCES

Achtemeier G. L., 1990: *The Use of Insects as Tracers for "Clear-Air" Boundary-Layer Studies by Doppler Radar. J. Atmos. Oceanic Tech.*, **8**, 746-765.

Ackerman, T. P., and G. Stokes, 2003: The Atmospheric Radiation Measurement program, *Phys. Today*, **56**, 38-45.

Clothiaux, E. E., T. P. Ackerman, G. G. Mace, K. P. Moran, R. T. Marchand, M. A. Miller, B. E. Martner, 2000: Objective determination of cloud heights and radar refectivities using a combination of active remote sensors at the ARM CART sites. *J. Appl. Meteor.*, **39**, 645-665.

Frisch, A.S., C.W. Fairall and J.B. Snider, 1995: Measurement of stratus cloud and drizzle parameters in ASTEX with a Kα –band Doppler radar and microwave radiometer. *J. Atmos. Sci.*, **52**, 2788-2799

Geerts, B., Q. Miao, 2005: The Use of Millimeter Doppler Radar Echoes to Estimate Vertical Air Velocities in the Fair-Weather Convective Boundary Layer, *J. Atmos. Oceanic Technol.*, **22**, 225-246.

Gossard, E.E., J.B. Snider, E.E. Clothiaux, B. Martner, J.S. Gibson, R.A. Kropfli, and A.S. Frisch, 1997: The potential of 8-mm radars for remotely sensing cloud drop size distributions. J. Atmos. OceanicTechnol., **14**, 76-87.

Hildebrand, P. H. and R. S. Sekhon, 1974: Objective Determination of the Noise Level in Doppler Spectra, *Journal of Applied Meteorology*, **13**, 808–811

Hogan, R. J., N. Gaussiat, and A. J. Illingworth, 2005: Stratocumulus Liquid Water Content from Dual-Wavelength Radar. *J. Atmos. Oceanic Tech.,* **22**, 1207-1218

Jordan, J. R., R.J. Lataitis and D.A. Carter, 1997: Removing ground and intermittent clutter contamination from wind profiler signals using wavelet transforms. *J. Atmos. Oceanic Technol.* **14**, 1280–1297.

Khandwalla, A., S. M. Sekelsky, and M. Quante, 2003: Algorithms for Filtering Insect Echoes from Cloud Radar Measurements. In Proceedings of the *Thirteenth ARM Science Team Meeting Proceedings, Broomfield, Colorado, March 31-April 4.*

Khandwalla, A., N. Majurec, S. M. Sekelsky, C. R. Williams and K. S. Gage, 2002: Characterization of Radar Boundary Layer Data Collected During the 2001 Multi-Frequency Radar IOP. In Proceedings of the *Twelfth ARM Science Team Meeting Proceedings, St. Petersburg, Florida, April 8-12..*

Khandwalla, A, S. Sekelsky, L. Li, and M. Bergada, 2001: Theory and observations between Ka-band and W-band to explain scattering differences between insects. In *Proceedings of the Eleventh Atmospheric Radiation Measurement (ARM) Science Team Meeting. ARM-CONF-2001.*

Kollias, P., E. E. Clothiaux, M. A. Miller, B. A. Albrecht, G. L. Stephens and T. P. Ackerman, 2006a: Millimeter-Wavelength Radars – New Frontier in Atmospheric Cloud and Precipitation Research. *Submitted to Bulletin Amer. Meteor. Soc.*

Kollias, P., E. E. Clothiaux, M. A. Miller, E. Luke, K. L. Johnson, K. P. Moran, K. B. Widener, and B. A. Albrecht, 2007: The Atmospheric Radiation Measurement Program Cloud Profiling Radars: Second Generation Sampling Strategies, Processing, and Cloud Data Products. *J. Oceanic Atmos. Technol*.

Kollias, P., E. E. Clothiaux, B. A. Albrecht, M. A. Miller, K. P. Moran and K. L. Johnson, 2005: The Atmospheric Radiation Measurement Program Cloud Profiling Radars. An Evaluation of Signal Processing and Sampling Strategies. *J. Atmos. Oceanic Techn.* **22**, 7, 930–948. doi: 10.1175/JTECH1749.1

Kollias, P., B.A. Albrecht, R. Lhermitte, and A. Savtchenko, 2001: Radar observations of updrafts, downdrafts, and turbulence in fair weather cumuli. *J. Atmos. Sci.* **58***,* 1750–1766.

Kosko, B., 1992: *Neural Networks and Systems: A Dynamical Systems Approach to Machine Intelligence.* Prentice Hall, 449 pp.

Lhermitte R., 1987: A 94 GHz Doppler radar for clouds observations. *J. Atmos. Oceanic Technol*., **4**, 36-48.

Lhermitte, R. M., 1966: Probing air motion by Doppler analysis of radar clear air returns. *J. Atmos. Sci.,* **23,** 575–591.

Long, CN, DW Slater, and T Tooman. 2001. Total Sky Imager Model 880 Status and Testing Results. ARM Technical Report ARM TR-006, U.S. Department of Energy, Washington, D.C.

Mead J. B. and K. Widener, 2005: W-band ARM Cloud Radar. Preprints, *32th Int. Conf. on Radar Meteorology*, Amer. Meteor. Soc., Albuquerque, NM.

Moran, K. P., B. E. Martner, M. J. Post, R. A. Kropfli, D. C. Welsh, and K. B. Widener, 1998: An unattended cloud-profiling radar for use in climate research. *Bull. Amer. Meteor. Soc.*, **79**, 443-455.

Morse, Corinne S., R. K. Goodrich, L. B. Cornman, 2002: The NIMA Method for Improved Moment Estimation from Doppler Spectra *J. Atmos. Oceanic Tech.*, **19**, 274-295

Sekelsky, S. M., L. Li, J. Calloway, R. E. McIntosh, M. A. Miller, E. E. Clothiaux, S. Haimov, G. Mace, and K. Sassen, 1998: Comparison of millimeter-wave cloud radar measurements for the fall 1997 cloud IOP. In *Proceedings of the Eighth Atmospheric Radiation Measurement (ARM) Science Team Meeting*, DOE/ER-0738, pp. 671-675.

Stokes, G. M., and S. E. Schwartz, 1994: The Atmospheric Radiation Measurement (ARM) Program: Programmatic Background and Design of the Cloud and Radiation Test Bed. *Bull Amer. Meteor. Soc.*, **75**, 1201-1222.

Vaughn, C. R. 1985. Birds and insects as radar targets: a review. *Proc. IEEE*. **73**: 205-227.

Wilson, J. W., T. M. Weckwerth, J. Vivekanandan, R. M. Wakimoto, and R. W. Russell. 1994. Boundary layer clear-air radar echoes: origin of echoes and accuracy of derived winds. *J. Atmos. Ocean. Tech*. **11**, 1184 -1206.

9. TABLES

Temp. (°C)	Date		Temp. (°C)	Date
0	1/10/2006		11	3/17/2006
1	3/22/2006		12	12/10/2005
2	2/16/2006		13	12/25/2005
3	1/20/2006		14	2/1/2006
4	12/16/2005		15	12/11/2005
5	3/19/2006		16	4/3/2006
6	2/12/2006		17	3/27/2006
7	1/17/2006		18	12/29/2005
8	3/24/2006		19	3/15/2006
9	1/13/2006		20	4/19/2006
10	3/25/2006			

Table 1. The set of twenty one temperature bins ranging from 0 °C to 20 ºC and their associated dates used to develop the model between surface temperature and insect coverage, as shown by the plot in figure 3b.

training class	samples	date
clear	2000	2/21/05
cloud	2000	2/21/05
precip	2000	2/21/05
insects	2000	3/28/05

Table 2. Number of data samples and their dates of occurrence for each class used to train the insect clutter detection algorithm.

10. FIGURE CAPTIONS

Figure 1. Example of MMCR radar reflectivity on a clear (cloud-free) day at the SGP ACRF. The layer of insect returns near the surface exhibits significant diurnal variability in intensity and vertical extent.

Figure 2. Hourly average surface temperature at 60 m and hourly average insect column height for May 2005. The Pearson correlation coefficient between average temperature and average insect column height is 0.92. Insect column height is defined as the highest range gate containing at least 50% insect returns during a 15 minute interval.

Figure 3. (a) Time-series of insect column height (dotted line) based on the insect classifier mask and the 10 °C isotherm height (solid line) derived from the soundings for May 2005. (b) The fractional insect coverage averaged over the 2nd and 3rd MMCR range gates (with centers at 150 m and 195 m) as a function of the temperature at 25 m altitude. Superimposed is the sigmoid logistic curve (shaded thick line) that models the observations reasonably well. (c) The mean Doppler velocity distribution of insect radar returns.

Figure 4. (a--h) Examples of insect-generated MMCR Doppler spectra at the SGP ACRF. The fundamental morphology is a sharp narrow peak, as shown in a). It is not difficult to visualize a)—h) as composed of scaled super-positions of a). Despite their great diversity, we have found insect clutter in the SGPACRF MMCR to contain

consistently spiked sub-peaks with sharp roll-offs.

Figure 5. Two curves providing evidence that occurrence of multi-peaked insect spectra is heavily biased toward high insect density time-height neighborhoods compared to single-peaked spectra. This leads us to speculate that, at least to some extent, spectral peaks can be mapped to individual insects. Here, insect return density is defined as the fraction of range gates within a 5 by 5 time-height neighbourhood.

Figure 6. (a) Doppler spectra-based insect detection algorithm main functional blocks. (b) Expanded view of the various modules of the feature extractor and the neural network. Pv is the input power spectrum of the primary peak, LPF is a smoothing filter, H1 and H2 are spectral derivative frequency distribution accumulators, σ is the spectral width, <V> is the mean Doppler velocity, K(V) is kurtosis, S(V) is skewness, r is range, JD is day of the year, and "winner" is the winner-takes-all decision criterion.

Figure 7. (a) Examples of insect (left) and cloud (right) MMCR Doppler spectra. (b) Insect (left) and cloud (right) primary Doppler spectra peaks after noise floor thresholding. (c) Insect (left) and cloud (right) primary Doppler spectra peak first derivatives. (d) Insect (left) and cloud (right) primary Doppler spectra peak second derivatives. (e) Histogram of first derivatives for the insect (left) and cloud (right) Doppler spectra primary peaks. (f) Histogram of second derivatives for the insect (left) and cloud (right) Doppler spectra primary peaks.

Figure 8. (a) Frequency of occurrence histogram of MMCR CDR in the boundary layer for the full month of May 2005. (b) Frequency of occurrence histograms of MMCR CDR for insect and hydrometeor radar returns as labelled by the insect/hydrometeor classifier.

Figure 9. Accuracy of the insect classification as a function of primary Doppler spectra peak spectral width. For spectral widths less than 0.2 m s-1 the overwhelming probability is for the return to be from insects. This, plus the similar morphologies of narrow insect and narrow hydrometeor spectra makes identification of hydrometeor returns with narrow spectral widths difficult.

Figure 10. (a) Time-height mapping of MMCR radar reflectivity (0.0--5.3 km) for several days in May 2005. (b) Corresponding hydrometeor/insect classification mask produced by the Doppler spectra-based insect detection algorithm for the same period.

Figure 11. (a) Examples of MMCR reflectivities for mixtures of clouds and insects at the SGP ACRF. (b) The ARSCL cloud mask (green) and the ceilometer cloud base height (black line). (c) The hydrometeor/insect classification mask produced by the Doppler spectra-based insect detection algorithm for the same periods as in b). The ceilometer cloud base height, the black line in c), is not an input to the classifier. Blue represents range gates classified as hydrometeors and green to those initially classified as insect by the classifier that are changed to hydrometeor based on MMCR CDR measurements. Red indicates the presence of insect returns.

Figure 12. (a) Example of MMCR (35-GHz) insect returns at the SGP ACRF with (b) corresponding returns from the 94-GHz radar.

Figure 13. (a) Scatter plot of insect radar reflectivities at 35- and 94-GHz for May 19, 2006. (b) 94-GHz LDR frequency of occurrence distributions for May 21, 2006. For both curves in b) the left peak is from hydrometeors and the right is from insects. The solid curve is based on extracting the cloud mask from the co-polarized channel SNR, whereas the dotted curve is based on the cross-polarized SNR mask. The trade-off between sensitivity and class separability is evident, as the dotted curve shows better separability but is based on a more aggressive cloud mask with fewer overall returns.

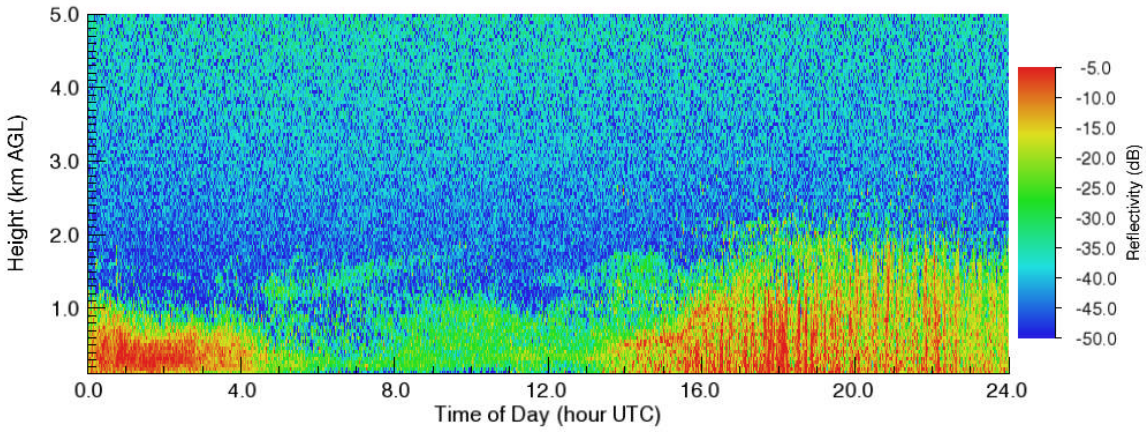

Figure 1. Example of MMCR radar reflectivity on a clear (cloud-free) day at the SGP ACRF. The layer of insect-returns near the surface exhibits significant diurnal variability in intensity and vertical extent.

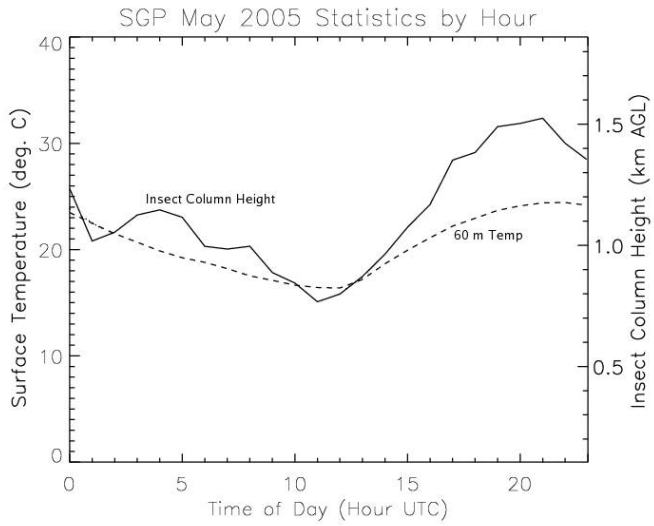

Figure 2. Hourly average surface temperatures at 60 m and hourly average insect column height for May 2005. The Pearson correlation coefficient between average temperature and average insect column height is 0.92. Insect column height is defined as the highest range gate containing at least 50% insect returns during a 15 minute interval.

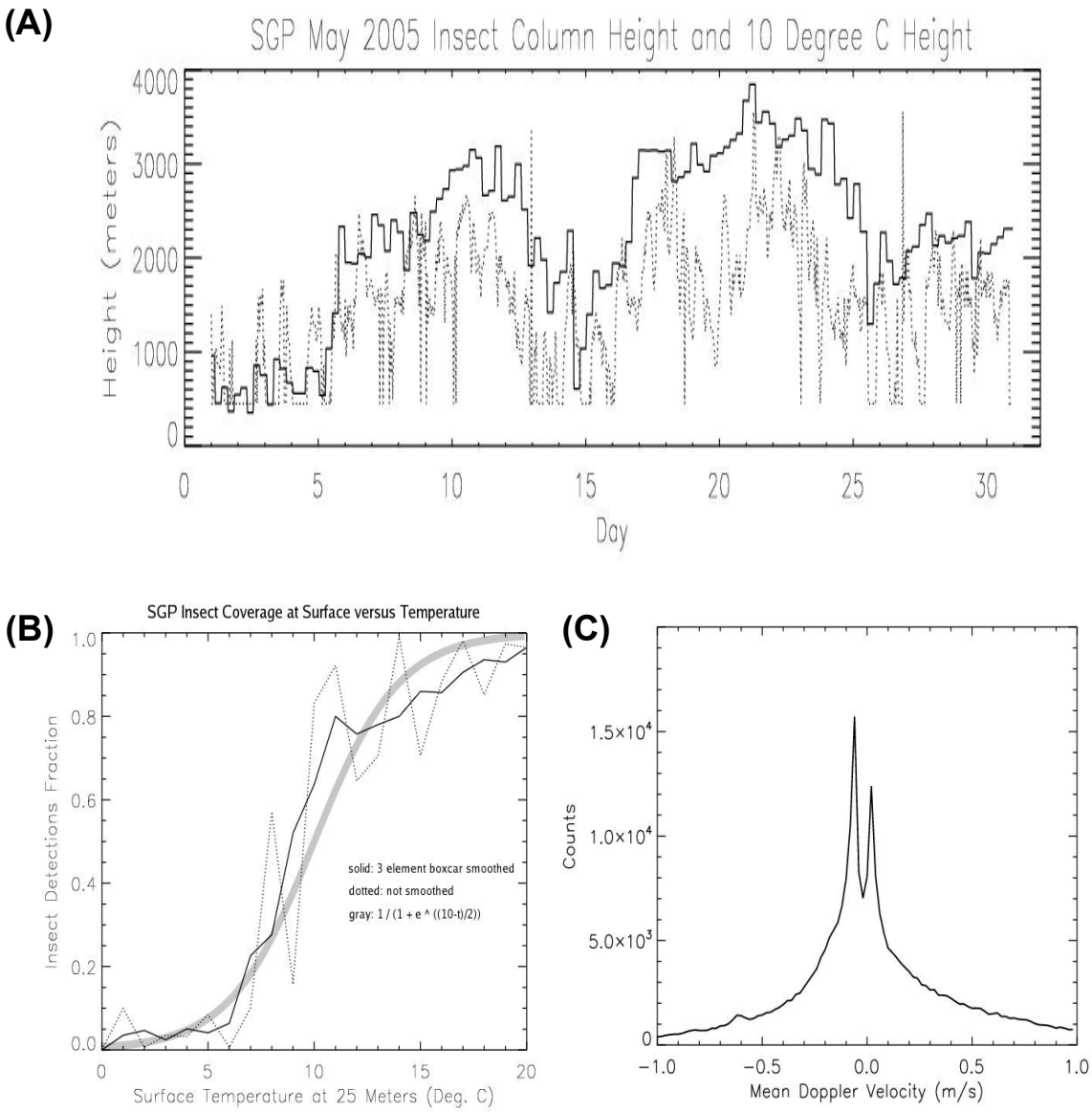

Figure 3. (a) Time-series of insect column height (dotted line) based on the insect classifier mask and the 10 °C isotherm height (solid line) derived from the soundings for May 2005. (b) The fractional insect coverage averaged over the 2nd and 3rd MMCR range gates (with centers at 150 m and 195 m) as a function of the temperature at 25 m altitude. Superimposed is the sigmoid logistic curve (shaded thick line) that models the observations reasonably well. (c) The mean Doppler velocity distribution of insect radar returns. Again, the insect layer height is estimated as the highest range gate averaging at least 50% insect returns during a 15 minute interval.

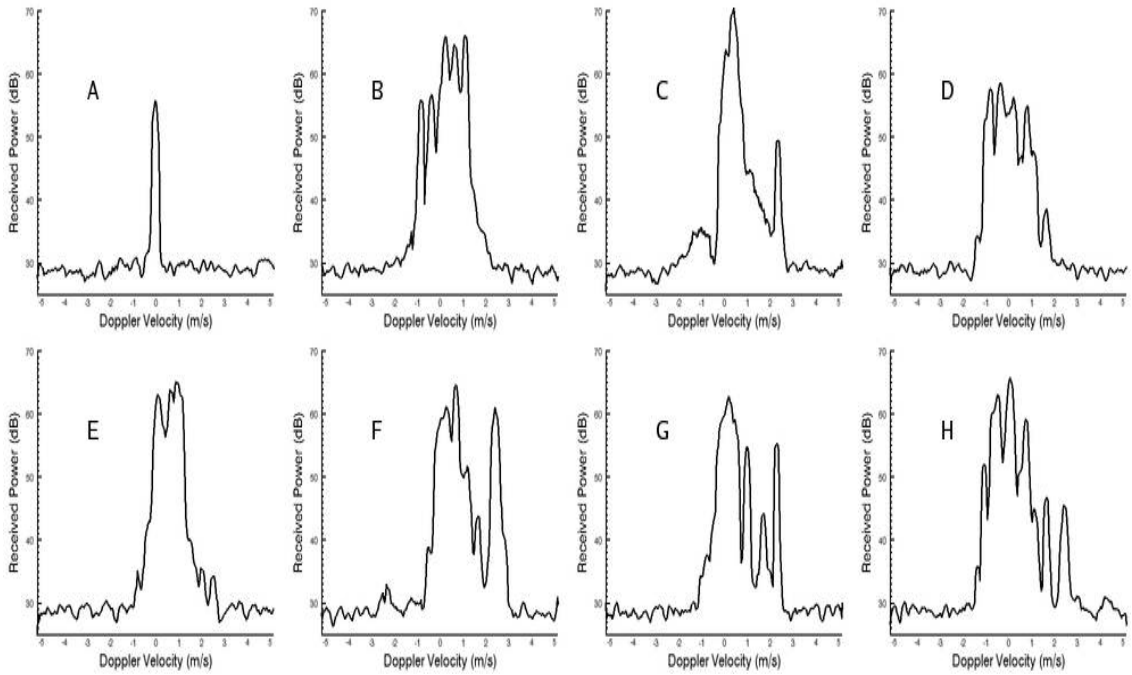

Figure 4. (a--h) Examples of insect-generated MMCR Doppler spectra at the SGP ACRF. The fundamental morphology is a sharp narrow peak, as shown in a). It is not difficult to visualize a)—h) as composed of scaled super-positions of a). Despite their great diversity, we have found insect clutter in the SGPACRF MMCR to contain consistently spiked sub-peaks with sharp roll-offs.

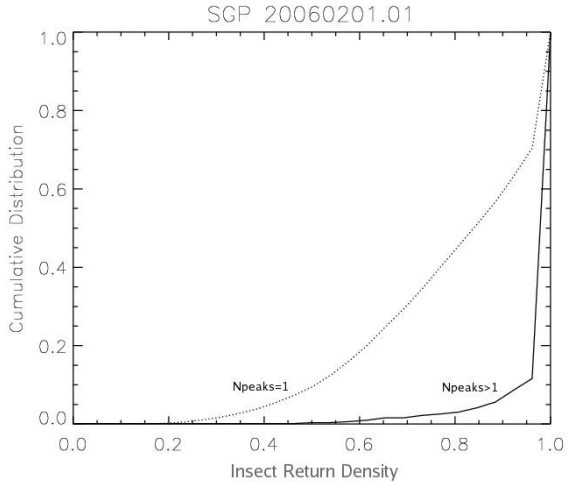

Figure 5. Two curves providing evidence that occurrence of multi-peaked insect spectra is heavily biased toward high insect density time-height neighborhoods compared to single-peaked spectra. This leads us to speculate that, at least to some extent, spectral peaks can be mapped to individual insects. Here, insect return density is defined as the fraction of range gates containing insects within a 5x5 local time-height neighbourhood.

(A)

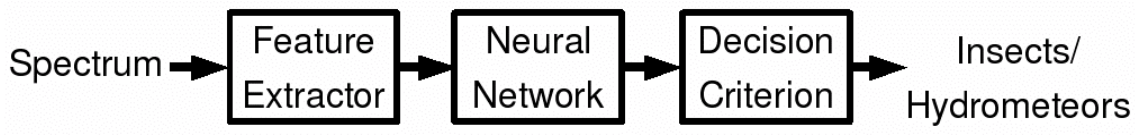

(B)

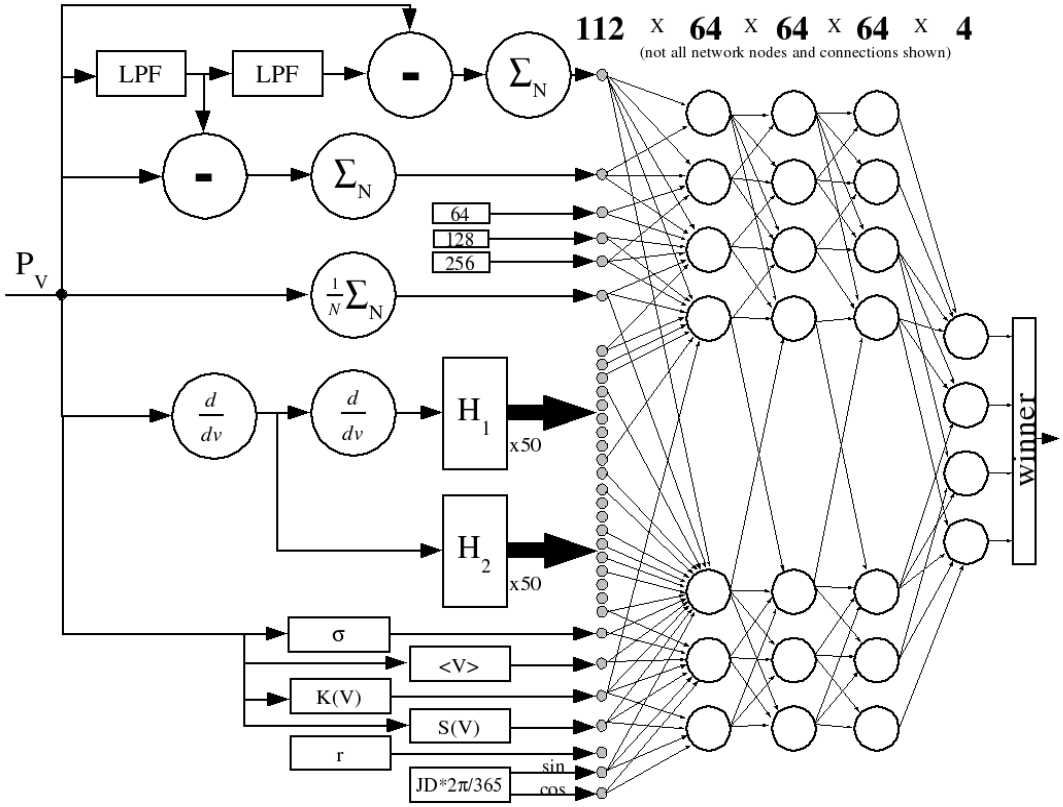

Figure 6. (a) Doppler spectra-based insect detection algorithm main functional blocks. (b) Expanded view of the various modules of the feature extractor and the neural network. Pv is the input power spectrum of the primary peak, LPF is a smoothing filter, H1 and H2 are spectral derivative frequency distribution accumulators, σ is the spectral width, <V> is the mean Doppler velocity, K(V) is kurtosis, S(V) is skewness, r is range, JD is day of the year, and "winner" is the winner-takes-all decision criterion.

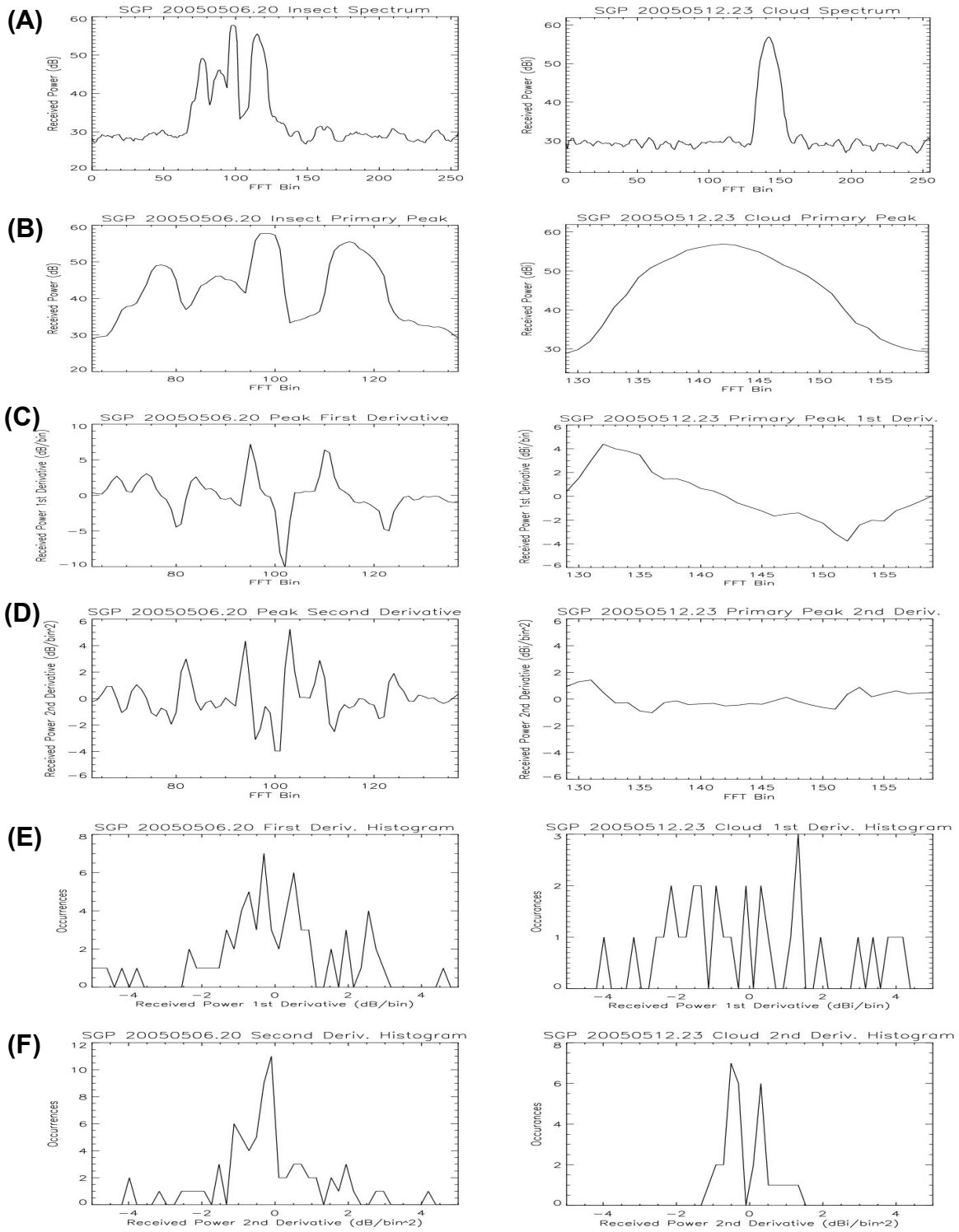

Figure 7. (a) Examples of insect (left) and cloud (right) MMCR Doppler spectra. (b) Insect (left) and cloud (right) primary Doppler spectra peaks after noise floor thresholding. (c) Insect (left) and cloud (right) primary Doppler spectra peak first derivatives. (d) Insect (left) and cloud (right) primary Doppler spectra peak second derivatives. (e) Histogram of first derivatives for the insect (left) and cloud (right) Doppler spectra primary peaks. (f) Histogram of second derivatives for the insect (left) and cloud (right) Doppler spectra primary peaks.

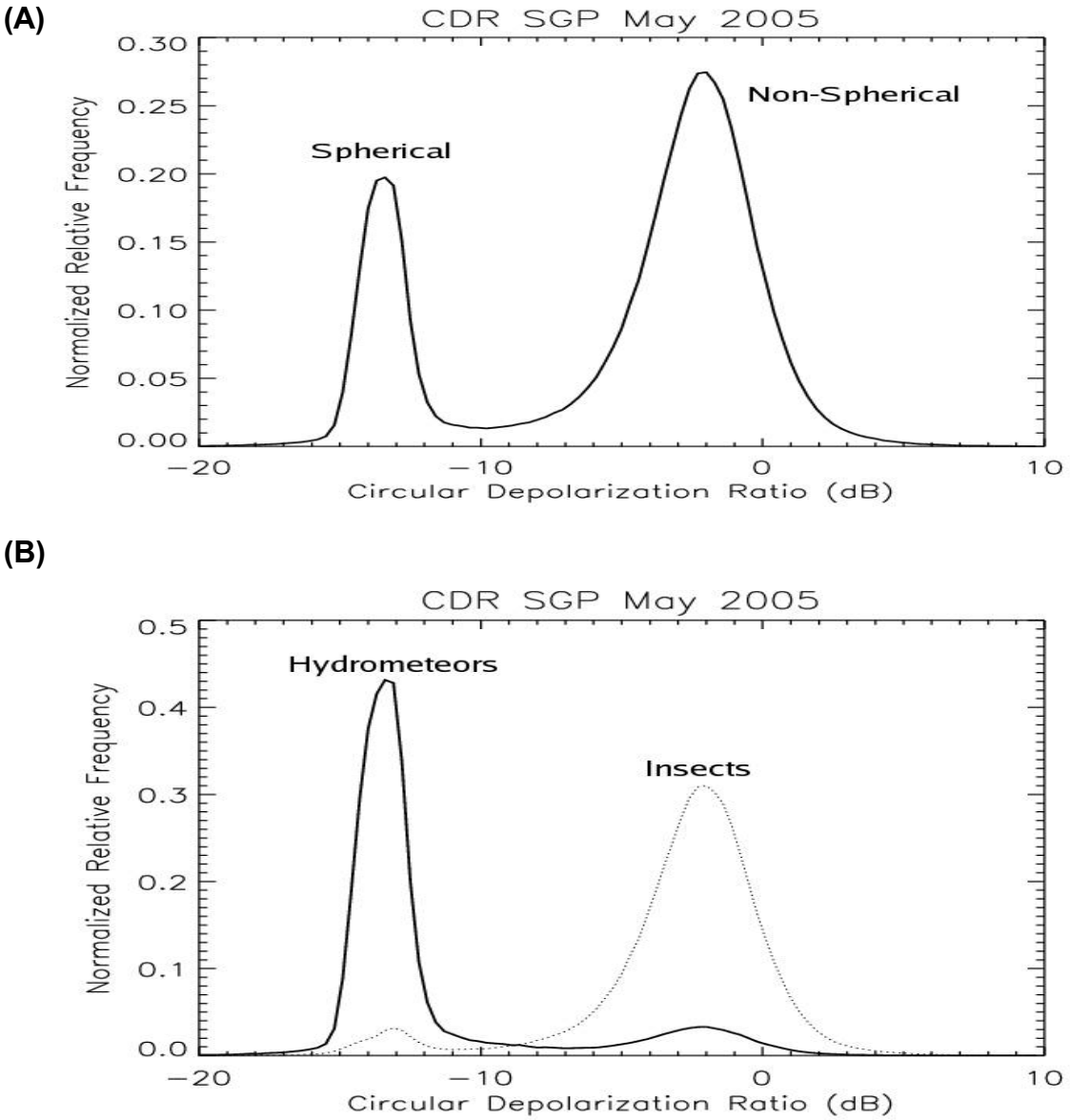

Figure 8. (a) Frequency of occurrence histogram of MMCR CDR in the boundary layer for the full month of May 2005. (b) Frequency of occurrence histograms of MMCR CDR for insect and hydrometeor radar returns as labelled by the insect/hydrometeor classifier.

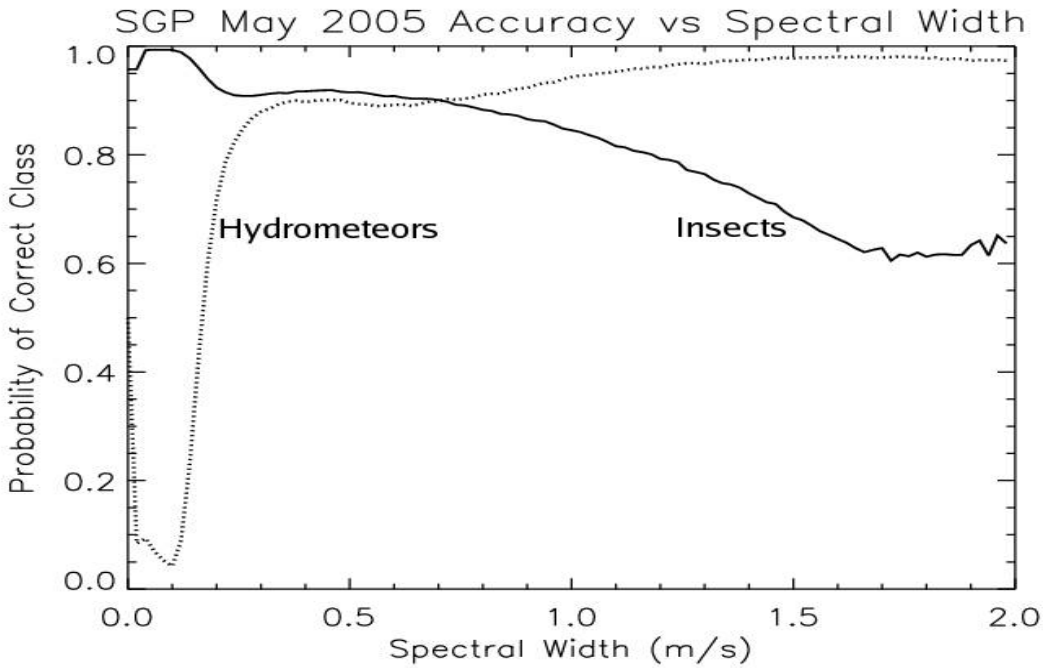

Figure 9. Accuracy of the insect classification as a function of primary Doppler spectra peak spectral width. For spectral widths less than 0.2 m s-1 the overwhelming probability is for the return to be from insects. This, plus the similar morphologies of narrow insect and narrow hydrometeor spectra makes identification of hydrometeor returns with narrow spectral widths difficult.

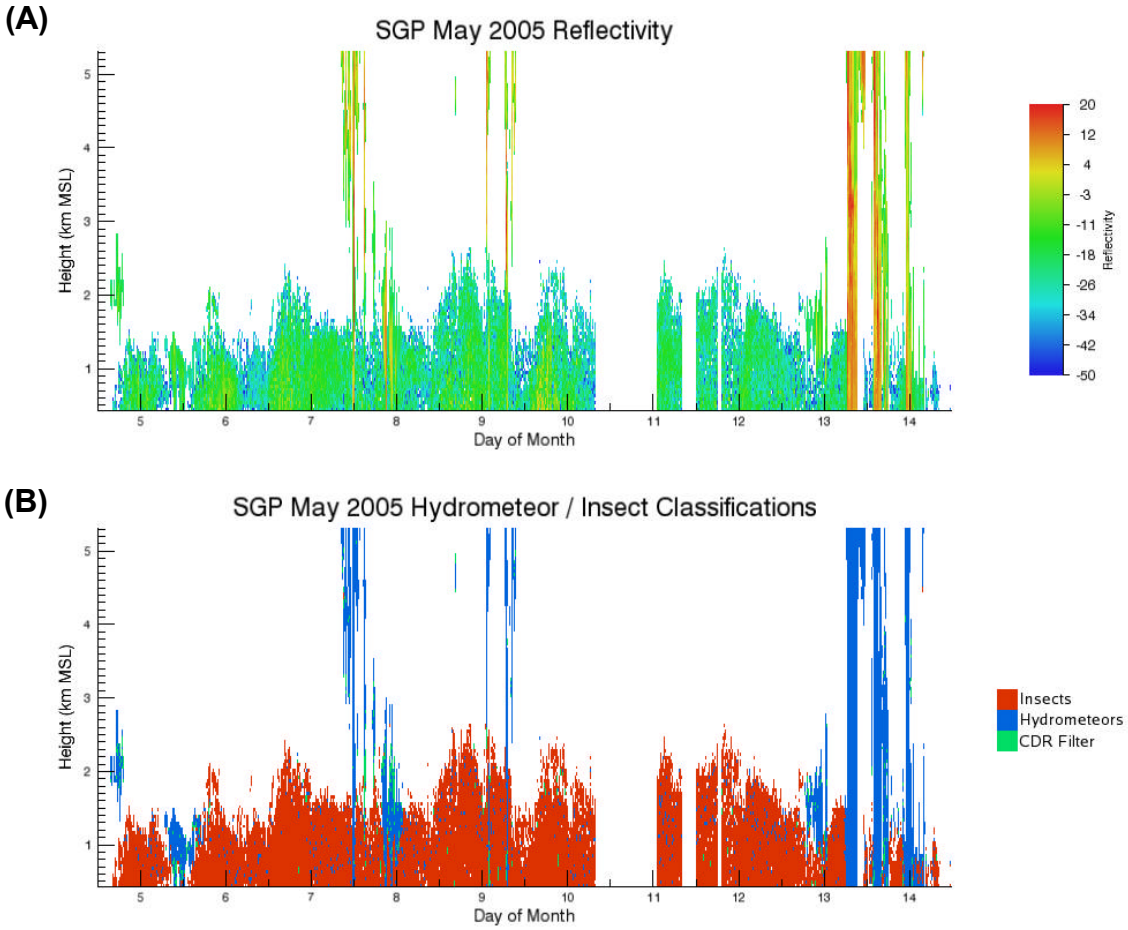

Figure 10. (a) Time-height mapping of MMCR radar reflectivity (0.0--5.3 km) for several days in May 2005. (b) Corresponding hydrometeor/insect classification mask produced by the Doppler spectra-based insect detection algorithm for the same period.

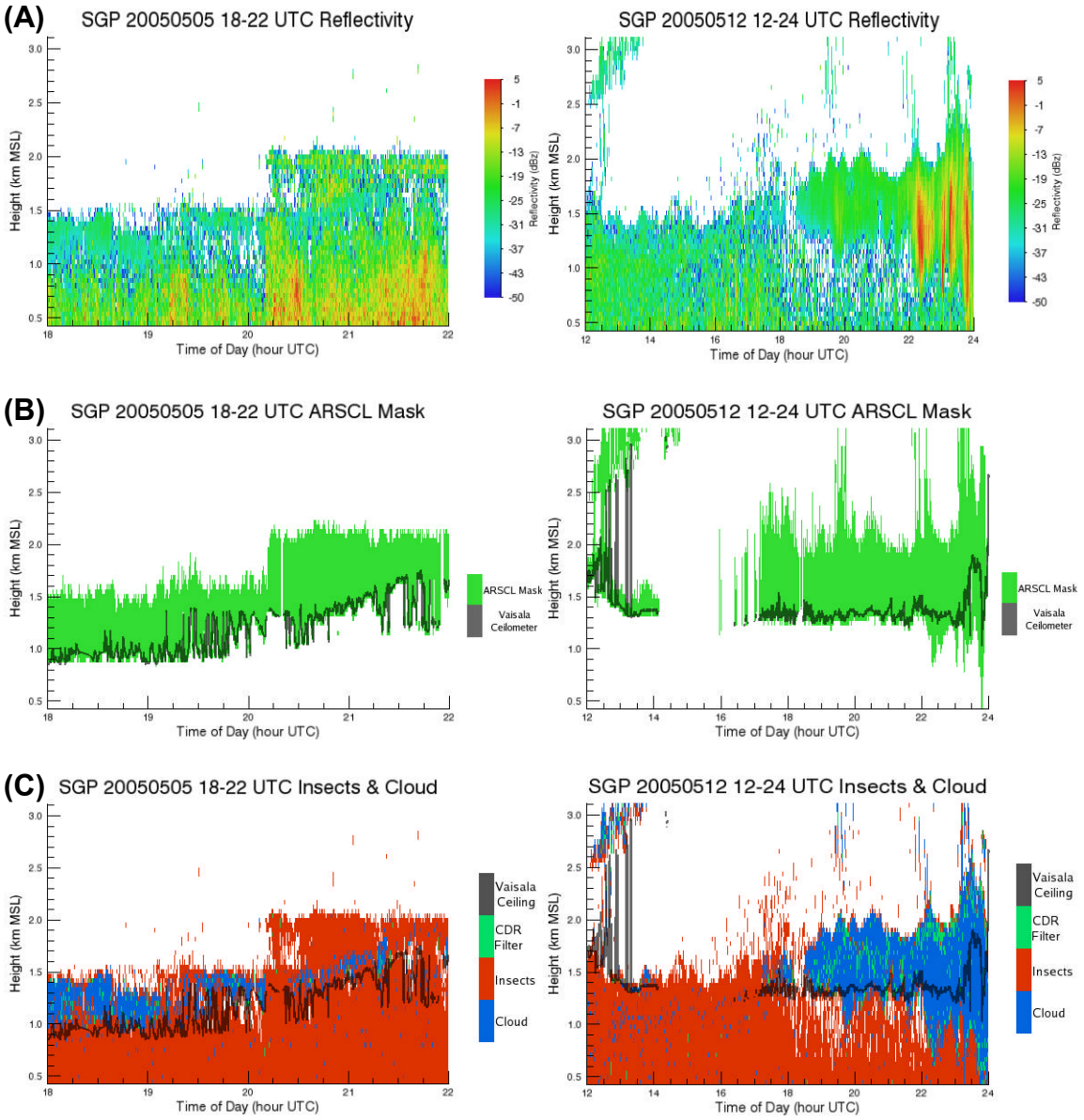

Figure 11. (a) Examples of MMCR reflectivities for mixtures of clouds and insects at the SGP ACRF. (b) The ARSCL cloud mask (green) and the ceilometer cloud base height (black line). (c) The hydrometeor/insect classification mask produced by the Doppler spectra-based insect detection algorithm for the same periods as in b). The ceilometer cloud base height, the black line in c), is not an input to the classifier. Blue represents range gates classified as hydrometeors and green to those initially classified as insect by the classifier that are changed to hydrometeor based on MMCR CDR measurements. Red indicates the presence of insect returns.

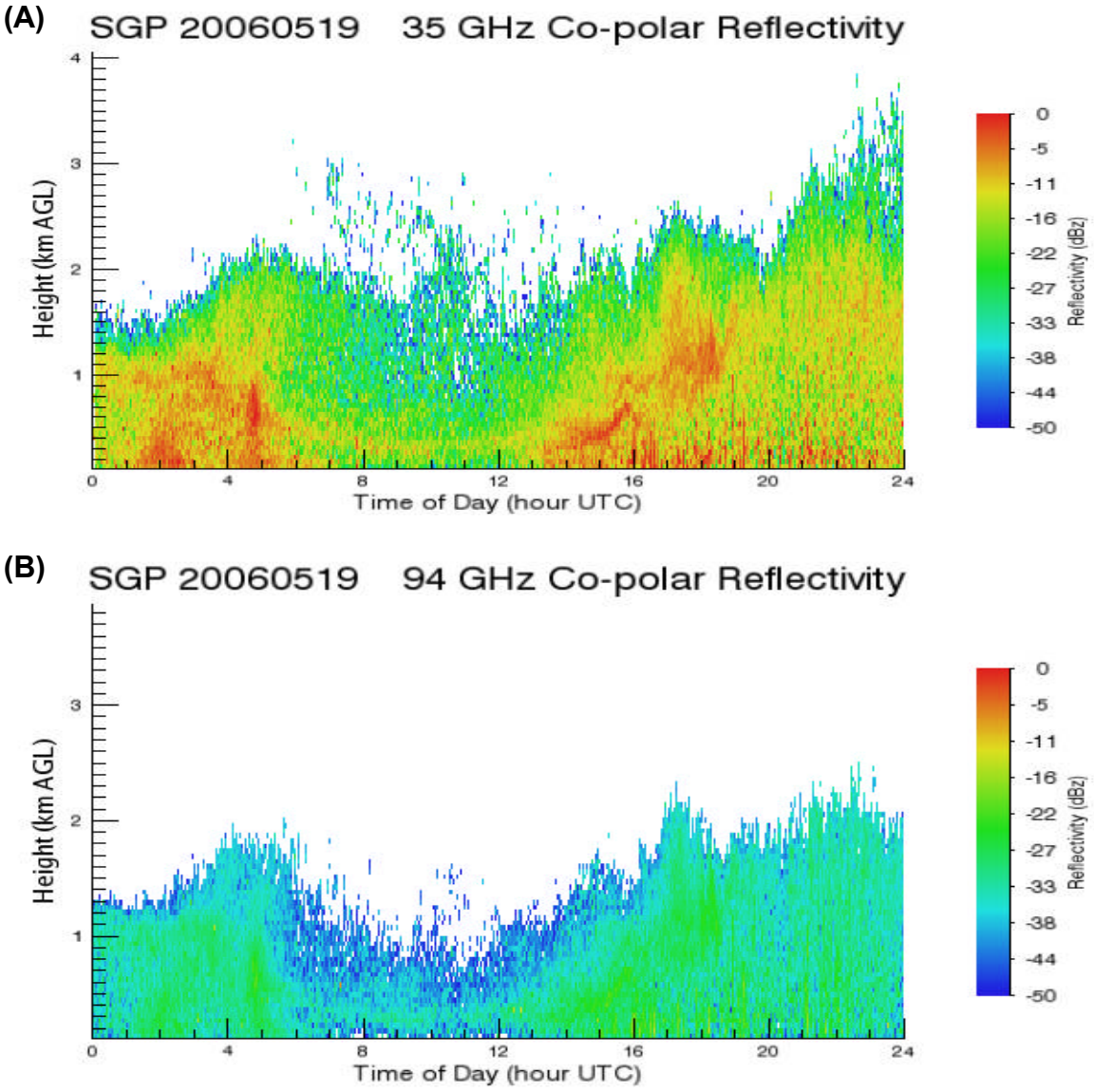

Figure 12. (a) Example of MMCR (35-GHz) insect returns at the SGP ACRF with (b) corresponding returns from the 94-GHz radar.

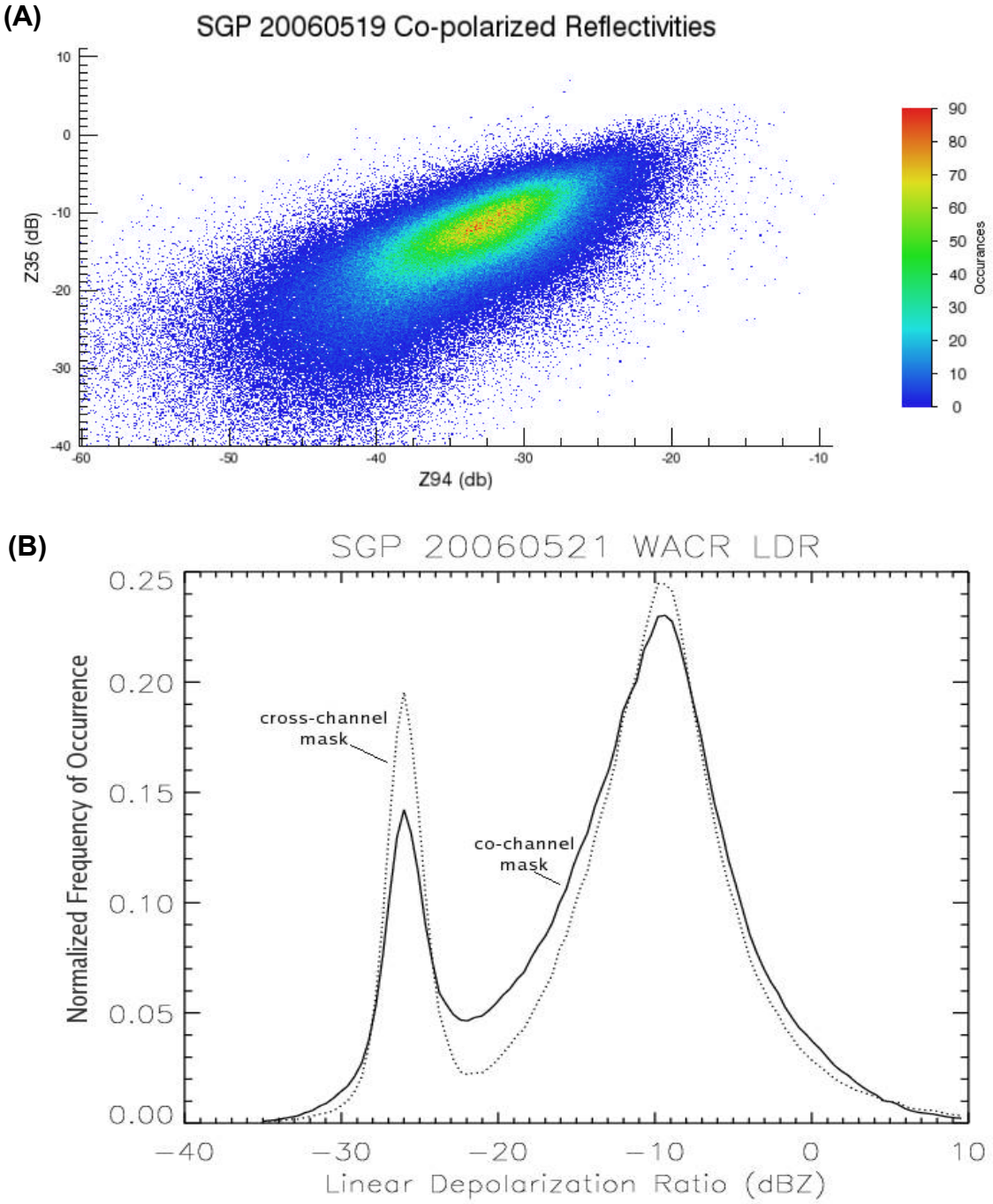

Figure 13. (a) Scatter plot of insect radar reflectivities at 35- and 94-GHz for May 19, 2006. (b) 94-GHz LDR frequency of occurrence distributions for May 21, 2006. For both curves in b) the left peak is from hydrometeors and the right is from insects. The solid curve is based on extracting the cloud mask from the co-polarized channel SNR, whereas the dotted curve is based on the cross-polarized SNR mask. The trade-off between sensitivity and class separability is evident, as the dotted curve shows better separability but is based on a more aggressive cloud mask with fewer overall returns.